


## RESEARCH ARTICLE

# Interplay between bone marrow adiposity and bone resorption in RANKL-mediated modelled osteoporosis

Vagelis Rinotas<sup>1</sup> | Evi Gkikopoulou<sup>1,2</sup> | Efthymios Tzortzis<sup>1,2</sup> |  
Konstantinos Kritikos<sup>1,2</sup> | Panagiota Siatra<sup>1,2</sup> | Apostolos Papadopoulos<sup>1,2</sup> |  
Vasiliki-Iris Perivolidi<sup>1,2</sup> | Eleni Douni<sup>1,2</sup> 

<sup>1</sup>Institute for Bioinnovation, Biomedical Sciences Research Center "Alexander Fleming", Vari, Greece

<sup>2</sup>Laboratory of Genetics, Department of Biotechnology, Agricultural University of Athens, Athens, Greece

**Correspondence**

Eleni Douni, Laboratory of Genetics, Department of Biotechnology, Agricultural University of Athens, Iera Odos 75, 11855 Athens, Greece; Institute for Bioinnovation, Biomedical Sciences Research Center "Alexander Fleming", Fleming 34, 16672, Vari, Greece.  
Email: [douni@aua.gr](mailto:douni@aua.gr) and [douni@fleming.gr](mailto:douni@fleming.gr)

**Funding information**

This research has been co-financed by the European Union and Greek national funds through the Operational Program Competitiveness, Entrepreneurship and Innovation under the call RESEARCH—CREATE—INNOVATE (Project code: T1EDK-02829). The publication of the article in OA mode was financially supported by HEAL-Link

**Abstract**

Bone marrow adipose tissue (BMAT) accrues in osteoporosis, whereas its contribution to the progression of bone resorption remains insufficiently understood. To understand the mechanisms that promote BMAT expansion in osteoporosis, in the present study, we performed extensive analysis of the spatiotemporal pattern of BMAT expansion during the progression of bone resorption in TgRANKL transgenic mouse models of osteoporosis expressing human RANKL (receptor activator of nuclear factor- $\kappa$ B ligand). Our results showed that TgRANKL mice of both sexes developed dramatically increased BMAT expansion compared to wild-type (WT) littermates, that was analogous to the levels of RANKL expression and the severity of the bone loss phenotype. BMAT was formed at close proximity to areas undergoing active bone remodelling and bone resorption, whereas bone resorption preceded BMAT development. Expression analysis in bone fractions demonstrated that BMAT constitutes a major source for RANKL production. Ex vivo analysis of isolated bone marrow stromal cells from TgRANKL mice showed an increased adipogenic differentiation capacity compared to WT, while osteoclast supernatants further exaggerated adipogenesis, supporting a critical role of the osteoclast-derived secretome in the differentiation of bone marrow adipocytes. Furthermore, the effectiveness of an antiosteoporosis treatment in BMAT development was investigated upon treatment of TgRANKL models with the bisphosphonate alendronate. Notably, alendronate effectively improved bone mass and attenuated BMAT expansion, indicating a possible involvement of osteoclasts and bone resorption in BMAT development. On the contrary, inhibition of BMAT with PPAR $\gamma$  antagonists (GW9662 or BADGE) effectively ameliorated BMAT expansion but failed to reverse the osteoporotic phenotype of TgRANKL mice. Overall, our data demonstrate that TgRANKL mice constitute unique genetic mouse models for investigating the pathogenic mechanisms that regulate the development and expansion of BMAT in osteolytic diseases.

**KEYWORDS**

animal models, bone marrow adiposity, osteoclast, osteoporosis, RANKL

This is an open access article under the terms of the [Creative Commons Attribution-NonCommercial-NoDerivs](https://creativecommons.org/licenses/by-nc-nd/4.0/) License, which permits use and distribution in any medium, provided the original work is properly cited, the use is non-commercial and no modifications or adaptations are made.

© 2024 The Author(s). *Journal of Cellular Physiology* published by Wiley Periodicals LLC.

## 1 | INTRODUCTION

During adult life, bone integrity is maintained through a coordinated process known as bone remodelling that enables the removal of the old and damaged bone through a continuous balanced interplay between the activities of osteoclasts and osteoblasts which either resorb or synthesise the extracellular bone matrix, respectively (Karsenty & Wagner, 2002). Increased bone remodelling rates caused by overwhelming osteoclast activity result in bone loss disorders including osteoporosis, which is characterised by low bone mass, and decreased bone mineral density (BMD) leading to reduced bone strength and increased risk of fractures (Gullberg et al., 1997). Receptor activator of nuclear factor- $\kappa$ B ligand (RANKL) constitutes the major mediator of osteoclast formation inducing bone resorption (Fuller et al., 1998; Lacey et al., 1998). RANKL functions through its cognate receptor RANK and can be inhibited by the decoy soluble receptor osteoprotegerin (OPG) that counterbalances the effects of RANKL by antagonising its binding to RANK receptor, while the RANKL/OPG ratio has been used as a biomarker for bone resorptive diseases (Bucay et al., 1998; Marcadet et al., 2022).

Bone marrow adipose tissue (BMAT) was considered until recently as a space filler of empty bone marrow (BM) areas following reduced hematopoiesis during aging. However, recent advances emerged BM adipocytes (BMAd) as a metabolically active heterogeneous cell population that interacts with the hematopoietic cells and the surrounding bone (Tratwal et al., 2021). BMAd originate from skeletal stem cells (SSCs), a multipotent self-renewing subset of BM stromal cells (BMSCs) (Abdallah & Kassem, 2012), and can occupy more than 70% of the BM space in older individuals, while this proportion increases in conditions including obesity, diabetes, anorexia nervosa and osteoporosis (Rendina-Ruedy & Rosen, 2020). It has been previously shown that under bone loss conditions, the differentiation of SSCs favours adipogenesis over osteogenesis (Rosen & Bouxsein, 2006). Even though postmenopausal osteoporosis patients present with high BM adiposity (BMA) (Li, Xu, Chen, et al., 2014) and BMAd respond to antiosteoporotic treatments (Duque et al., 2011; Yang et al., 2015), the role of BMAT in the regulation of bone homeostasis and bone resorption remains poorly understood. The dynamics of BMAd in bone resorption has been investigated in mouse models of bone loss, demonstrating also a negative association between BMAT and BMD (Beekman, Zwaagstra, et al., 2019; Li et al., 2023), while the underlying mechanism remain compelling. We have previously generated transgenic mice expressing human RANKL (huRANKL) using as a transgene a 200 kb genomic fragment that includes the coding region and regulatory sites of the *huRankl* gene (Rinotas et al., 2014). This results in a physiologically relevant overexpression pattern of the *huRankl* gene, which mirrors the expression pattern of the endogenous mouse *Rankl* gene. Overexpression of *huRankl* in TgRANKL mice results in increased bone turnover, trabecular bone loss, cortical porosity as well as increased BMAT formation (Rinotas et al., 2014), modelling osteolytic diseases such as hereditary familial juvenile Paget's disease and osteoporosis. In the current study, we investigated the development and progression of BMAT in the TgRANKL mouse models. Furthermore, we investigated through preclinical studies in TgRANKL mice, the effect of alendronate

(ALN), an inhibitor of osteoclast activity, in BMAT accumulation and reversely the effect of inhibitors of adipogenesis in the progression of osteoporosis, to get insights about the mechanistic interplay between bone resorption and BMAT formation.

## 2 | MATERIALS AND METHODS

### 2.1 | Mouse husbandry

TgRANKL mice (Tg5516 and Tg5519 lines) (Rinotas et al., 2014), were maintained and bred under specific pathogen-free conditions in the animal facility of Biomedical Sciences Research Centre "Alexander Fleming."

### 2.2 | Microtomographic ( $\mu$ CT) analysis

Femurs were fixed in 10% neutral-buffered formalin (Carlo Erba Reagents) overnight at 4°C. The next day the femurs were washed and stored in phosphate-buffered saline (PBS). The microarchitecture of the distal femurs was evaluated using a high-resolution X-ray  $\mu$ CT scanner (SkyScan1172, Bruker). Images were acquired at 50 KeV, 100  $\mu$ A with a 0.5 mm aluminum filter. Three-dimensional reconstructions (8.8  $\mu$ m cubic resolution) were generated using NRecon software (Bruker). Femoral trabecular geometry was assessed using 300 continuous CT slices (1800  $\mu$ m) located at the trabecular area underneath the growth plate. The trabecular area of the distal femur bones was assessed through the bone volume fraction (BV/TV, %), the trabecular number (Tb.N,  $\text{mm}^{-1}$ ), the trabecular separation (Tb.S, mm), the trabecular thickness (Tb.Th, mm) and the BMD ( $\text{g}/\text{cm}^3$ ). Femoral cortical geometry was assessed using 100 continuous CT slides (600  $\mu$ m) located at the femoral midshaft, while the parameters measured included the cortical bone volume fraction (Ct.BV/TV, %), the cortical bone volume (Ct.BV,  $\text{mm}^3$ ), the tissue volume (TV,  $\text{mm}^3$ ), the BM volume ( $\text{mm}^3$ ), the cortical thickness (Ct.Th, mm), the total cortical porosity (Po(tot), %) and the tissue mineral density ( $\text{g}/\text{cm}^3$ ) (Bouxsein et al., 2010).

### 2.3 | Quantitation of BMAT by osmium tetroxide staining and $\mu$ CT

Femur bones were stained with osmium tetroxide, as previously reported (Scheller et al., 2014), incorporating a few modifications. Briefly, bones were fixed for 24 h in 10% neutral-buffered formalin at 4°C, and subsequently they were washed with tap water and were decalcified in 13% EDTA, pH 7.4, for 14 days with one change. After washing with tap water for 2 h, 500  $\mu$ L of 1% osmium tetroxide solution (Electron Microscopy Services) was added to each femur placed in a 1.5-mL microtube. Bones were stained in the fume hood for 5 days at room temperature with two intermediate changes of freshly made osmium tetroxide solution. Osmium solution was carefully removed and decontaminated to a small liquid waste

container that had been filled with corn oil. Bones were transferred into embedded cassettes and washed under tap water for 3 h at room temperature. Each femur was then transferred to a new 1.5 mL microtube containing 1 mL PBS buffer and proceeded for  $\mu$ CT scanning. Quantitation of BMAT is depicted as adipose volume per marrow volume (Ad.V/Ma.V,%) (Bravenboer et al., 2020).

## 2.4 | BMAT isolation

BMAT was isolated from Tg5519 and wild-type (WT) littermates as previously described (Fan et al., 2017). In brief, for each mouse both femurs and tibiae were collected, cleaned in sterile PBS and snipped at both ends. Bones were placed in a 0.5-mL microtube that was cut at the bottom. The 0.5-mL tube was inserted into a 1.5-mL microtube containing 200  $\mu$ L of Dulbecco's Modified Eagle Medium (DMEM) medium. Fresh BM was spun out by quick centrifuge (till 10,000 rpm, 9 s) at room temperature. Floating adipocytes were collected from the top layer, while BM cells accumulated at the bottom of the 1.5-mL tube. Flushed femurs, adipocytes and BM cells were subsequently used for RNA analysis.

## 2.5 | Isolation of BMSCs, adipocyte differentiation and oil red staining

BMSC populations were isolated as previously described (Ghali et al., 2015). Briefly, femurs and tibiae were flushed and BM cells were dissociated through needles G21, G23 and G25 (three times per needle). Then, BM cells were seeded in 24-well plates at a density of  $4 \times 10^4$  per well. After incubation for 24 h at 37°C, nonadherent cells were discarded by rinsing with PBS. The attached cells were cultured with DMEM supplemented with 15% fetal bovine serum (FBS) (Biosera), 2 mM L-glutamine, 100 U/mL penicillin and 100 g/mL streptomycin (Gibco-Thermo Fisher Scientific) in a humidified incubator of 5% CO<sub>2</sub> at 37°C, and the culture media was changed every 2 days. At a confluency of 80%–90%, BMSCs were incubated with the DMEM adipogenic medium (Gibco-Thermo Fisher Scientific) supplemented with 10% FBS, 10  $\mu$ g/mL insulin, 0.1  $\mu$ M dexamethasone, 100  $\mu$ M indomethacin and 500  $\mu$ M 3-isobutyl-1-methylxanthine (Sigma-Aldrich) for 4 days. BMSCs were subsequently maintained in 10  $\mu$ g/mL insulin, 0.1  $\mu$ M dexamethasone and 5  $\mu$ M pioglitazone for 10 days and the medium was changed every 2 or 3 days. Cells were fixed in 2% paraformaldehyde for 15 min, washed with water, incubated with 60% isopropanol for 5 min and stained with newly filtered oil red O solution (SERVA Electrophoresis GmbH) for 10 min at room temperature. Adipocytes were counted under inverted microscope (Zeiss).

## 2.6 | Adipogenic differentiation of BMSCs under osteoclast-conditioned medium (OCM)

RAW264.7 cells were plated in 6-well plates at a density of  $6 \times 10^4$  cells per well and cultured in osteoclastogenic medium containing

a-MEM medium (Gibco-Thermo Fisher Scientific), 10% FBS and 40 ng/mL GST-RANKL (Douni et al., 2012). The osteoclastogenic medium was replenished after 2 days. On the 4th day of osteoclastogenesis, the medium was replaced with serum-free DMEM (Gibco-Thermo Fisher Scientific) for 24 h. Supernatants were collected upon centrifugation at 450g for 5 min, while they were stored at  $-80^{\circ}\text{C}$  until use. The co-culture experiments were performed with some modifications as previously described (Zhang et al., 2018). At a confluency of 80%–90%, BMSCs were incubated with a mixture of DMEM adipogenic medium (20% FBS, 2 mM L-glutamine, 100 U/mL penicillin and 100 g/mL streptomycin, 0.1  $\mu$ M dexamethasone, 100  $\mu$ M indomethacin and 500  $\mu$ M 3-isobutyl-1-methylxanthine) and DMEM osteoclast conditional medium from differentiated RAW264.7 cells (1:1 v/v ratio) for 4 days. BMSCs were subsequently maintained in a mixture of DMEM adipogenic medium (20% FBS, 2 mM L-glutamine, 100 U/mL penicillin and 100 g/mL streptomycin, 10  $\mu$ g/mL insulin, 0.1  $\mu$ M dexamethasone and 5  $\mu$ M pioglitazone) and DMEM osteoclast conditional medium (1:1 v/v ratio) for 10 days and the mixture medium was changed every 2 or 3 days.

## 2.7 | RNA isolation and quantitative real-time PCR analysis

Total RNA was extracted from whole femurs and BMSCs using a monophasic solution of guanidine isothiocyanate and phenol according to the manufacturer's instructions (TRI Reagent; MRC). After the removal of DNA remnants with DNase I treatment (Sigma-Aldrich), first-strand cDNA was synthesised using 2  $\mu$ g of total RNA and M-MLV (Invitrogen). Templates were amplified with HOT FIRE-Pol<sup>®</sup> EvaGreen Master Mix (Solis Biodyne) on the CFX96 Connect real-time PCR instrument (Bio-Rad Laboratories). Data analysis was performed with reference to the  $2^{-\Delta\Delta C_t}$  method. A list of gene-specific primers (Eurofins Genomics) can be found in Supporting Information S1: Table S4. For each experiment, at least three biological and two technical replicates were used.

## 2.8 | Treatment of mice with ALN

ALN (Calbiochem cat. no. 126855) at the dose of 1 or 2 mg/kg was administered intraperitoneally in Tg5516 or the Tg5519 mice, respectively, twice per week from the 5th week of age for a period of 6 weeks. PBS was administered in control experimental groups. Body weight was recorded weekly for each mouse. At 11 weeks of age, all mice were euthanized, and the long bones were collected for  $\mu$ CT and RNA analysis. Each group contained 10 mice (five females and five males).

## 2.9 | GW9662 and BADGE treatment

5-week-old Tg5516 mice were treated intraperitoneally daily either with 1 mg/kg GW9662 (SantaCruz, sc-202641) or 30 mg/kg BADGE

(Sigma-Aldrich, cat.no. D3415) and 15% DMSO in PBS (vehicle) for 6 weeks. The dosing was adjusted according to daily body weight measures. Mice were euthanized and abdominal white adipose tissue was isolated and weighted. Femurs were collected for  $\mu$ CT analysis.

## 2.10 | Statistical analysis

All results are expressed as mean values  $\pm$  standard deviation. Statistical significance was assessed by one or two-way analysis of variance (ANOVA) and Tukey or Dunnett's post hoc test to compare means of multiple groups. Student's *t* test was performed to compare two groups. For all tests,  $p < 0.05$  was considered statistically significant, \* $p < 0.05$ , \*\* $p < 0.01$ , \*\*\* $p < 0.001$ .

## 3 | RESULTS

### 3.1 | Progression of BMAT in TgRANKL osteoporotic mice

We have previously shown that both TgRANKL lines, Tg5516 and Tg5519, develop mild and severe trabecular bone loss, respectively. The concomitant progression of bone loss and BMAT in the femurs of both TgRANKL osteoporotic models was quantified through sequential  $\mu$ CT. Analysis of the metaphyseal region revealed a remarkable trabecular bone loss in both transgenic lines from the second month of age (Figure 1a,b, Supporting Information S1: Figure S1, Table S1). More specifically, Tg5516 mice developed gradually trabecular bone loss, while complete loss of the trabecular bone was already evident at 2-month-old Tg5519 mice, compared to WT mice. Subsequently, the BMAT accumulation was assessed in the same area upon osmium tetroxide staining and  $\mu$ CT analysis. Our results revealed a progressive increase of BMAT in the metaphyseal area of both sexes of TgRANKL lines (Figure 1c,d) that was analogous to the trabecular bone loss severity. Notably, by the 4th month of age most of the metaphyseal BM cavity was filled with BMAT in the severe osteoporotic model Tg5519.  $\mu$ CT analysis of the cortical bone at mid-diaphysis demonstrated a physiological architecture in Tg5516 mice, while Tg5519 mice developed cortical porosity by the second month of age (Figure 1e,f, Supporting Information S1: Table S1). Notably BMAT progressively accumulated only in the BM cavity of Tg5519 mice, whereas neither WT or Tg5516 mice developed BMAT at mid-diaphysis (Figure 1g,h). Collectively, these results demonstrated that in TgRANKL osteoporosis mouse models BMAT is formed in both sexes at close proximity to areas undergoing active bone remodelling and bone resorption.

Gene expression analysis with qPCR showed that the osteoclast-related genes *Dcstamp* and *Ctsk* as well as the osteogenic marker genes *Runx2*, *Alp* and *Ocn* were significantly upregulated in whole femurs from 4-month-old female Tg5519 mice compared to WT littermates and Tg5516 mice (Figure 2a,b), indicating increased bone turnover. Increased gene expression was also identified in adipogenic

markers including *Cebp/a*, *Pparg*, *Fabp4* and *Adiponectin* in Tg5519 femurs compared to WT (Figure 2c). However, in Tg5516 mice the above molecular biomarkers were not constantly upregulated compared to WT mice, indicating a milder bone turnover potential with moderate BMAT accumulation, in line with the  $\mu$ CT results (Figure 2). Altogether, these results confirm at the molecular level increased bone turnover and adipogenesis in TgRANKL mice.

### 3.2 | RANKL expression in BM, BMAT, flushed femurs, BMSCs and BMSC-derived adipocytes

We have previously shown that both mouse and human *Rankl* (*huRankl*) genes are highly expressed in the femurs of TgRANKL mice (Rinotas et al., 2014). To identify the major cellular source of RANKL, femurs were isolated from 4-month-old Tg5519 and WT mice, and subsequently were fractionated into BM, BMAT and flushed bones (Figure 2d) as previously described (Fan et al., 2017). The fractionation process was validated by the expression of cell-specific gene markers, confirming the expression of genes for osteoblasts (*Alp* and *Ocn*), osteocytes (*Sost*) and osteoclasts (*Ctsk*) in flushed bones, while adipogenic markers *Adiponectin* and *Fabp4* were expressed specifically in BMAT fractions (Figure 2e). Different primers were designed for mouse *Rankl* (*muRankl*) and *huRankl* genes to represent species specificity. The expression of *muRankl* was eightfold upregulated in BMAT and fivefold in bone compared to BM samples (Figure 2e). Similarly, *huRankl* followed the expression pattern of *muRankl*, displaying increased expression in BMAT and bone samples (Figure 2e).

Furthermore, we examined the expression of the transgene in undifferentiated BMSCs as well as in BMSC-derived adipocytes. Using a pair of primers that can detect total *Rankl* (human and mouse), we found that the BMSCs from Tg5519 mice expressed significantly higher levels of *Rankl* compared to WT (Supporting Information S1: Figure S2a). Since the BMSCs from Tg5519 and WT mice exhibit comparable expression levels of *muRankl* (Supporting Information S1: Figure S2a), the increased expression of total *Rankl* is attributed to the high expression levels of *huRankl* transgene. In addition, we observed an increased expression of *Pparg* in BMSCs derived from Tg5519 mice compared to WT (Supporting Information S1: Figure S2a). Comparing the expression of the transgene between undifferentiated BMSCs and BMSC-derived adipocytes we observed that the expression levels of *huRankl* were maintained, while the expression of the endogenous *muRankl* was downregulated upon differentiation (Supporting Information S1: Figure S2b).

### 3.3 | BMAT formation follows bone loss in Tg5519 mice

We then investigated whether BMAT formation precedes or follows bone resorption in the TgRANKL osteoporotic mouse models through  $\mu$ CT at various time points. In Tg5516 mice, both bone resorption and BMAT gradually progressed at the metaphyseal region from the 2nd

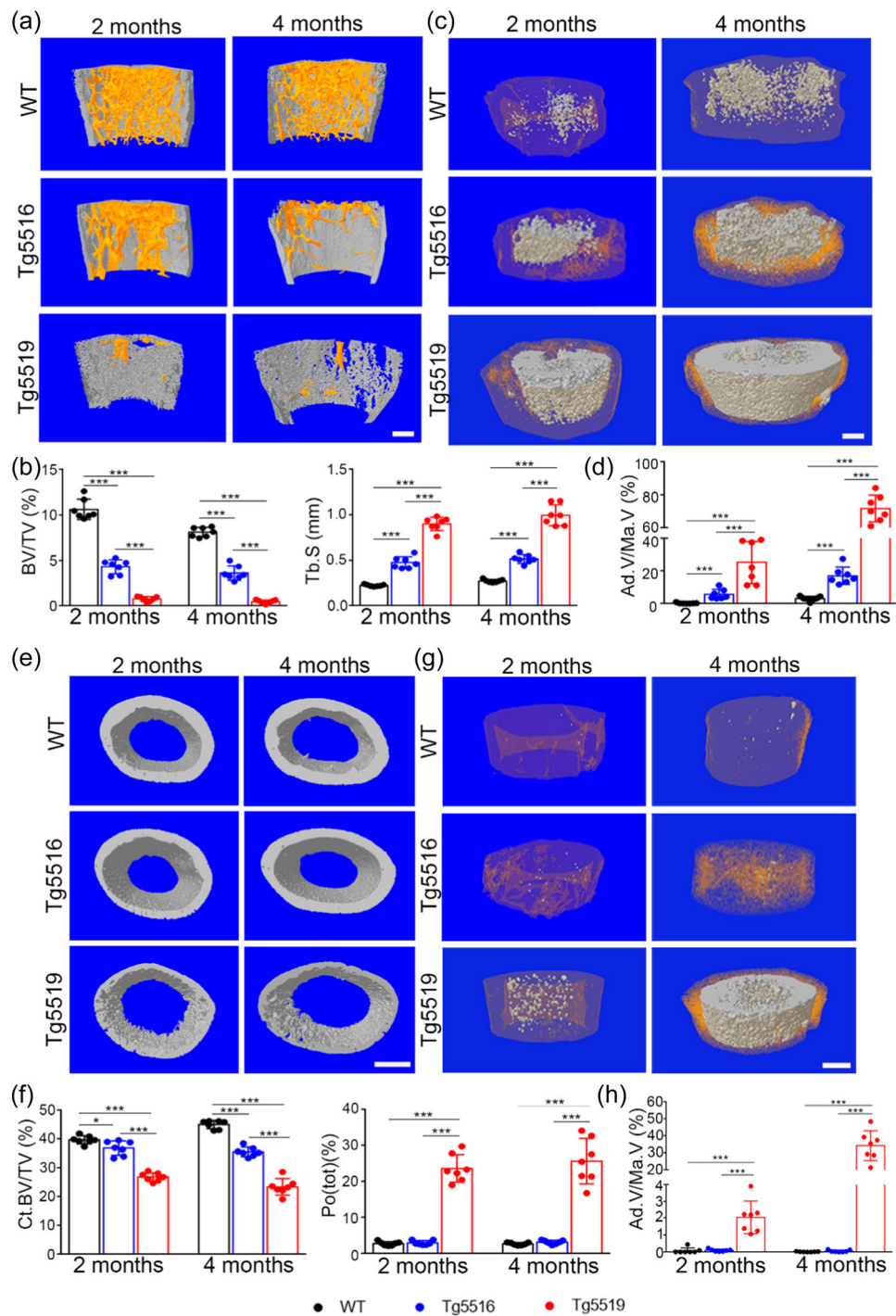


**FIGURE 1** Progression of trabecular bone loss, cortical porosity and bone marrow adipose tissue (BMAT) accumulation in distal femurs of 2- and 4-month-old female Tg5516, Tg5519 and wild-type littermates through microtomographic analysis. (a) Representative 3D reconstructed longitudinal images of trabecular (orange) and cortical bone (grey), at metaphysis (scale bar = 500  $\mu$ m) and (b) quantification of trabecular bone volume fraction (BV/TV, %) and separation (Tb.S). (c) Representative 3D reconstructed images of BMAT upon osmium staining at metaphyseal region (scale bar = 500  $\mu$ m) and (d) quantitation of BMAT with adipose volume fraction (Ad.V/Ma.V,%). (e) Representative 3D reconstructed cross-section images of the cortical bone (scale bar = 500  $\mu$ m) and (f) quantification of cortical bone volume fraction (Ct. BV/TV, %) and total porosity (Po(tot) %). (g) Representative 3D reconstructed images of BMAT (white) at midshaft, (scale bar = 300  $\mu$ m) and (h) quantitative analysis of adipose volume fraction (Ad.V/Ma.V,%). In plots (b), (d), (f) and (h) comparative statistical analysis was performed only among groups of the same age ( $n = 7$  per genotype). Data are shown as mean values  $\pm$  SD. One-way analysis of variance and Tukey post hoc test was performed for statistical analysis in groups of the same age. \* $p < 0.05$ , \*\*\* $p < 0.001$ .

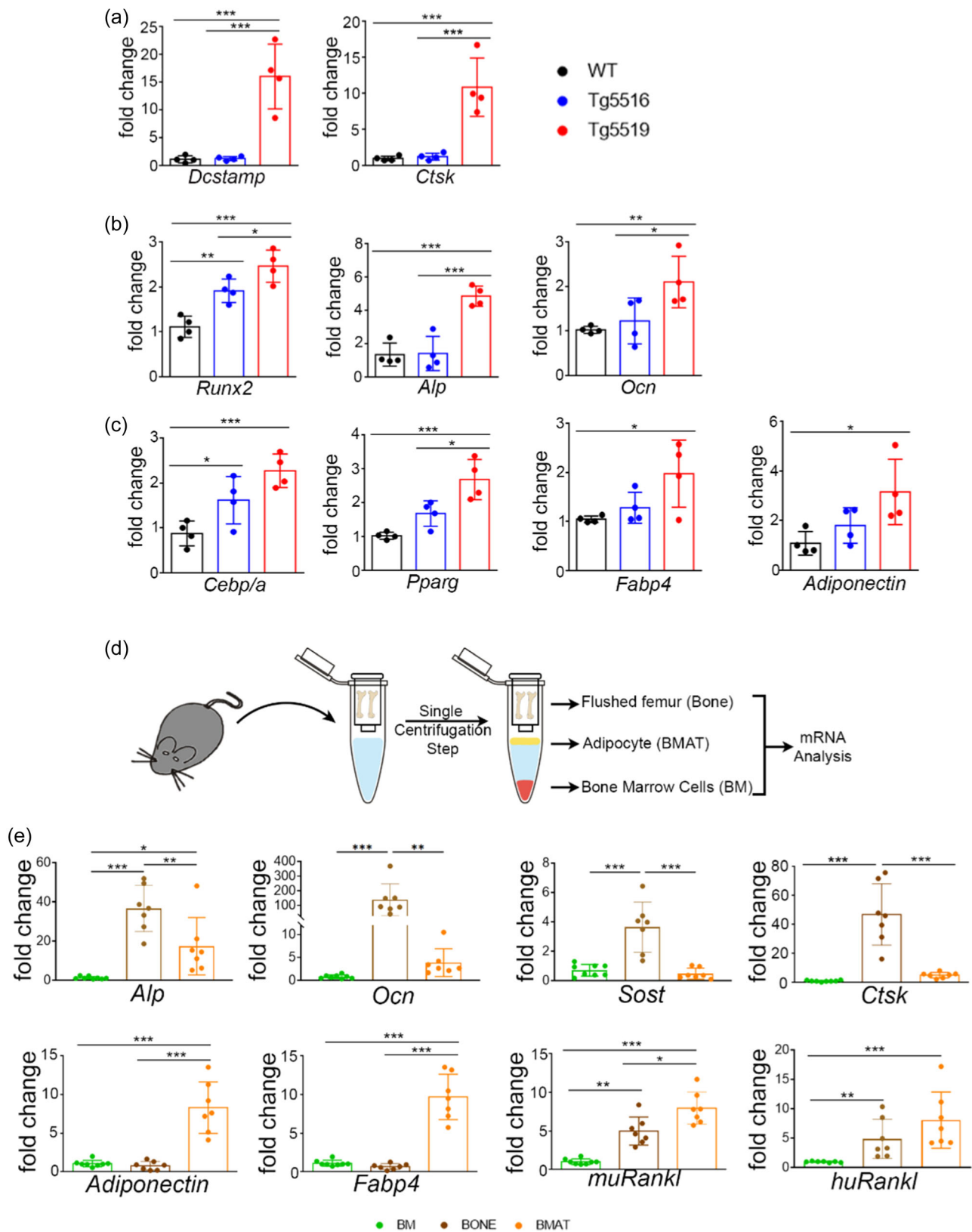


**FIGURE 2** Expression analysis in TgRANKL femurs. qPCR analysis in whole femurs from 4-month-old female Tg5516, Tg5519 and wild-type littermates ( $n = 4$  per genotype) for (a) osteoclast markers *Dcstamp*, and *Ctsk*, (b) osteogenic markers *Runx2*, *Alp* and *Ocn* and (c) adipogenic markers *Cebp/a*, *Pparg*, *Fabp4* and *Adiponectin*. (d) Schematic representation of the procedure used to isolate femoral fractions including BM, bone marrow adipose tissue and bones for qPCR analyses; (e) Comparative gene expression levels of markers for osteoblasts (*Alp*, *Ocn*), osteocytes (*Sost*), osteoclasts (*Ctsk*), adipocytes (*Adiponectin* and *Fabp4*), as well as for *muRankl*, and *huRankl* in fractionated samples from Tg5519 mice from both sexes ( $n = 7-8$ ). Relative fold change of expression was normalised against GAPDH. Data are shown as mean values  $\pm$  SD. One-way analysis of variance and Tukey post hoc test was performed for statistical analysis. \* $p < 0.05$ , \*\* $p < 0.01$ , \*\*\* $p < 0.001$ .

till the 8th month of age, while at 4 weeks of age, the structure of the femur was similar to that of WT mice without any signs of BMAT (Figure 3a–f). Even though trabecular bone loss and excessive cortical porosity were already established at 4-week-old Tg5519 mice (Figure 3a,c,d), BMAT was detectable after the 4th week of age (Figure 3b,e,f), suggesting bone resorption precedes BMAT formation. Furthermore, the expression of bone turnover-related genes (*Dcstmp*, *Ctsk* and *Runx2*) was significantly increased in femurs from 4-week-old Tg5519 mice compared to WT (Figure 3g), while the expression of adipogenic markers *Cebp/a*, *Pparg*, *Fabp4* and *Adiponectin* was similar to WT baseline levels (Figure 3h), supporting the phenotypic results. Taken together, our results indicate that BMAT formation follows bone loss in the Tg5519 osteoporosis model.

### 3.4 | BMSCs from TgRANKL mice display increased adipogenic potential

We then investigated whether increased BMAT formation in TgRANKL mice could be related with increased adipogenic potential of BMSCs. Indeed, BMSCs isolated from Tg5519 mice and cultured with adipogenic medium showed an increased adipogenic potential, with increased adipocyte numbers compared to WT BMSCs (Figure 4a,b). Interestingly, when BMSCs (either WT or Tg5519) differentiated toward adipogenesis in the presence of OCM (1:1 ratio), exaggerated adipogenesis was detected in both genotypes (Figure 4a,b), supporting a critical role of the osteoclast-derived secretome in BMAT differentiation. In addition, stimulation of BMSCs with OCM alone had no effect on adipocyte differentiation indicating that OCM is dispensable for adipogenesis (Figure 4a).

To investigate whether increased adipogenesis operates at the expense of osteogenesis, we performed osteogenic differentiation in BMSCs isolated from WT and Tg5519 mice. Our results showed significant reduction of the osteogenic potential of Tg5519 BMSCs compared to WT as shown by decreased deposition of extracellular calcium and quantitation of alizarin staining (Figure 4c–e).

### 3.5 | Pharmacological inhibition of bone resorption attenuates BMAT formation

To investigate the reciprocal interplay between bone resorption and BMAT formation, we first assessed BMAT progression upon pharmacological blockage of bone resorption. ALN, an antiresorptive bisphosphonate, was administered in TgRANKL mice intraperitoneally twice per week from the 5th week of age for a duration of 6 weeks. Tg5516 mice were treated prophylactically with 1 mg/kg of ALN, while the treatment of Tg5519 with 2 mg/kg ALN was therapeutic since the bone loss is already established at 4 weeks of age. PBS-treated WT and TgRANKL mice served as controls. Treatment of Tg5516 with ALN not only restored bone loss but also led to an increased expansion of the trabecular bone compared to WT mice as shown by  $\mu$ CT (Figure 5a,d, Supporting Information S1: Table S2) and

histological analysis (Supporting Information S1: Figure S3a). Notably, ALN treatment completely inhibited BMAT formation in Tg5516 mice (Figure 5b–d, Supporting Information S1: Table S2).

ALN administration in the severe osteoporosis model Tg5519 resulted in partial rescue of trabecular and cortical bone loss. At metaphysis, ALN treatment led to a thickening of the trabecular bone below the growth plate, whereas the trabecular bone failed to expand further into the marrow cavity in contrast to ALN-treated Tg5516 mice (Figure 5a,d, Supporting Information S1: Figure S3). BMAT formation was also partially attenuated in the metaphyseal area upon ALN treatment of Tg5519 mice (Figure 5b–d, Supporting Information S1: Table S2). At mid-diaphysis, the cortical bone volume fraction was restored but still the porosity in Tg5519 mice was not completely rescued (Figure 5e,f, Supporting Information S1: Table S2). Similarly, BMAT formation was partially inhibited in metaphysis and almost completely disappeared in mid-diaphysis upon ALN-treatment of Tg5519 mice compared to PBS-treated Tg5519 mice (Figure 5b–f, Supporting Information S1: Table S2). Conclusively, these results demonstrate that pharmaceutical inhibition of bone resorption abrogates BMAT formation in TgRANKL mouse models, further suggesting an involvement of osteoclasts in BM adipogenesis.

### 3.6 | Effect of pharmacological inhibition of adipogenesis in bone resorption

Further, we investigated whether inhibition of adipogenesis could ameliorate the mild osteoporotic phenotype of Tg5516 mice. For pharmacological inhibition of BMAT we used bisphenol A diglycidyl ether (BADGE) and GW9662, two known antagonists of PPAR $\gamma$  (Beekman, Veldhuis-Vlug, et al., 2019; Duque et al., 2013). Tg5516 mice were treated intraperitoneally daily either with 1 BADGE or 30 mg/kg GW9662 from the 5th week of age for a period of 6 weeks as previously published (Beekman, Zwaagstra, et al., 2019; Duque et al., 2013). Both compounds decreased the percentage of abdominal white fat compared to untreated mice, indicating their efficacy (Supporting Information S1: Figure S4). As expected, administration of BADGE or GW9662 resulted in a significant amelioration of BMAT expansion in Tg5516 mice (Figure 6a–d). More specifically, Tg5516 mice displayed approximately 70% reduction of adipocyte volume fraction upon treatment with GW9662 and BADGE compared to vehicle-treated Tg5516 littermates (Figure 6d, Supporting Information S1: Table S3). However, treatment with BADGE or GW9662 failed to rescue trabecular bone loss in Tg5516 mice (Figure 6c,e, Supporting Information S1: Table S3), indicating that BMAT is dispensable for bone resorption in this genetic model of osteoporosis.

## 4 | DISCUSSION

So far, the study of the gradual accumulation of BMAT in osteoporosis has been hampered due to the lack of appropriate in vivo models. In this study, we studied the progression of BMAT

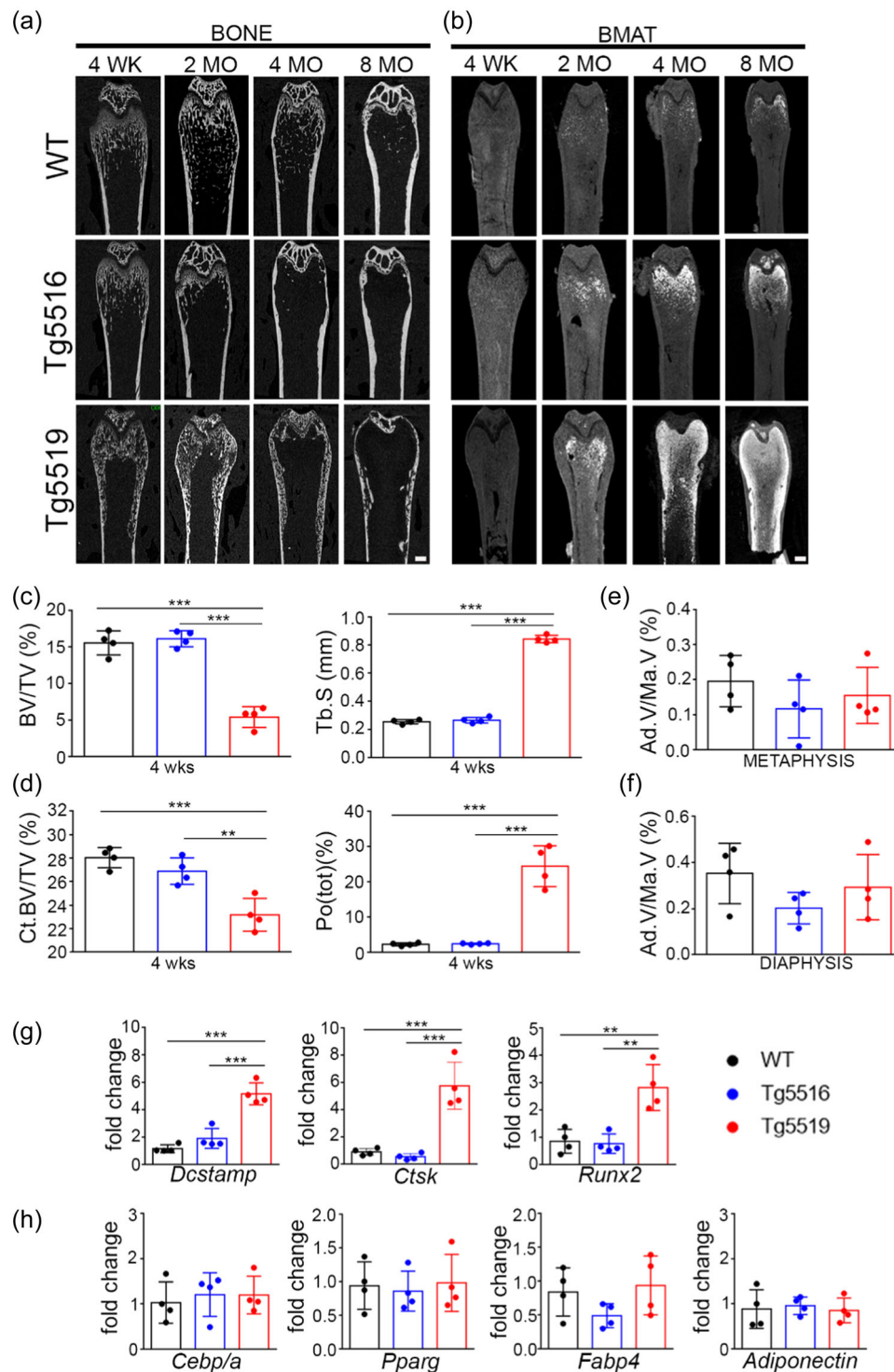


**FIGURE 3** Bone marrow adipose tissue (BMAT) expansion follows bone loss in Tg5519 mice. Representative longitudinal 2D microtomographic ( $\mu$ CT) reconstructions of distal femurs from female Tg5516, Tg5519 and wild-type (WT) littermates at different time points (4 weeks, 2 months, 4 months and 8 months) for (a) bone structure and (b) BMAT upon osmium tetroxide staining, scale bar = 500  $\mu$ m. Quantitative analysis of distal femurs from 4-week-old WT, Tg5516 and Tg5519 littermates with  $\mu$ CT analysis of (c) trabecular bone in the metaphyseal region for bone fraction (BV/TV, %) and separation (Tb.S), (d) cortical bone in the mid-diaphyseal region for cortical bone volume fraction (Ct.BV/TV, %) and total porosity (Po(tot) %). Adipose volume fraction (Ad.V/Ma.V, %) at (e) metaphysis and (f) mid-diaphysis at 4-week-old mice ( $n = 4$  per group). Comparative qPCR analysis in femurs from 4-week-old Tg5516, Tg5519 and WT littermate controls ( $n = 4$  per group) for (g) the bone turnover markers *Dcstamp*, *Ctsk* and *Runx2* and (h) the adipogenic markers *Pparg*, *Cebp/a*, *Fabp4* and *Adiponectin*. Relative fold change of expression was normalised against *GAPDH*. Data are shown as mean values  $\pm$  SD. One-way analysis of variance and Tukey post hoc test was performed for statistical analysis. \*\* $p < 0.01$ , \*\*\* $p < 0.001$ .



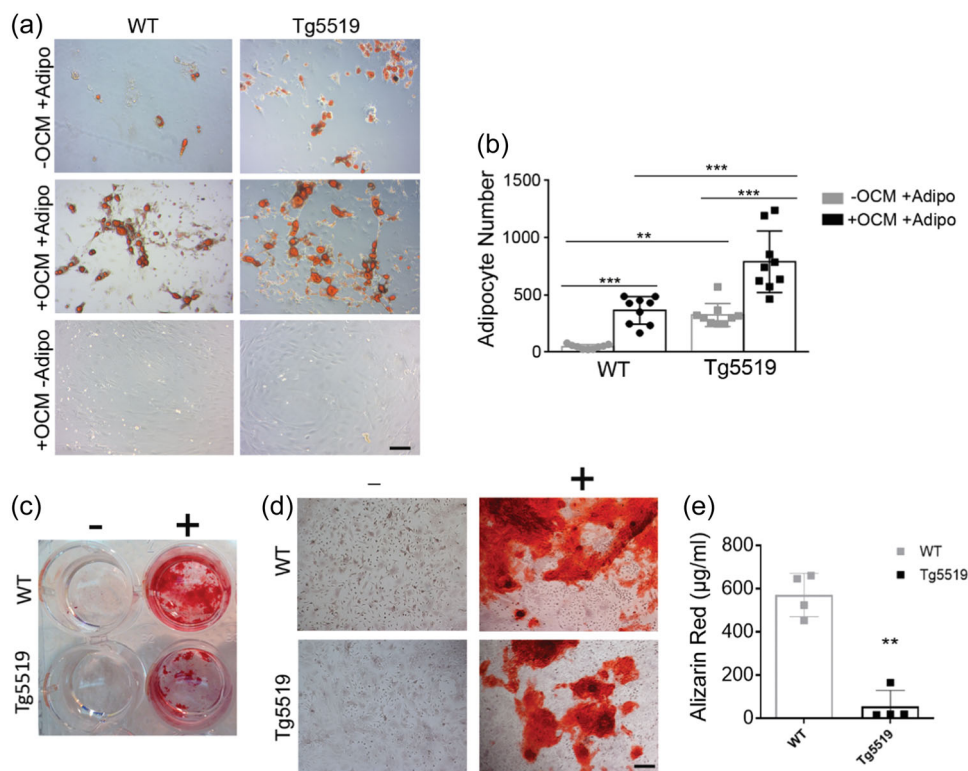


**FIGURE 4** Bone marrow stromal cells (BMSCs) from Tg5519 mice display increased adipogenic and decreased osteogenic potential while osteoclast supernatants further enhance adipogenesis. BMSC populations derived from 8-week-old wild-type (WT) and Tg5519 mice ( $n = 3$  per genotype), where cultured under adipogenic conditions for 14 days. (a) Representative Oil Red staining images demonstrating formation of lipid droplets after adipogenic differentiation of BMSCs derived from Tg5519 and WT controls treated with adipogenic cocktail (-OCM+Adipo), adipogenic cocktail supplemented with osteoclast-conditioned medium in 1:1 ratio (+OCM +Adipo) and with osteoclast-conditioned medium without adipogenic cocktail (+OCM -Adipo), scale bar = 100  $\mu\text{m}$ ; (b) Adipocyte number. Three independent experiments were performed ( $n = 3$  per group for each experiment). Data represent mean values  $\pm$  SD. Two-way analysis of variance and Tukey post-hoc test was performed. (c and d) Representative Alizarin O Red staining images demonstrating calcium deposition after 21 days of osteogenic differentiation of BMSCs from Tg5519 and WT controls, scale bar = 100  $\mu\text{m}$ ; (e) Quantification of Alizarin red staining. Two independent experiments were performed ( $n = 2$  mice per group for each experiment). Data represent mean values  $\pm$  SD. Student  $t$  test was performed.  $**p < 0.01$ ,  $***p < 0.001$ .

in osteoporotic TgRANKL mice expressing huRANKL (Rinotas et al., 2014), providing novel models of osteoporosis-related BMAT accumulation. Using  $\mu\text{CT}$  we managed to image and quantify in the same femur samples first the bone parameters and then upon osmium tetroxide staining the formation of BMAT in TgRANKL mice. The mild osteoporosis Tg5516 model gradually developed BMAT formation specifically at the metaphyseal region of distal femurs, a site with increased trabecular bone loss. A more pronounced and accelerated BMA phenotype developed in the severe osteoporosis Tg5519 model that displays both trabecular bone loss and cortical porosity. Notably, the formation of BMAT in both TgRANKL lines initiated at the metaphyseal area, which is characterised by bone loss, while it expanded towards diaphysis only in Tg5519 mice that develop cortical porosity. A similar pattern of BMAT expansion at regions of close proximity with bone loss has been previously reported in ovariectomized, OPG-deficient and aged mice (Iwaniec & Turner, 2013; Takeshita et al., 2014; Zhang et al., 2016). However, TgRANKL mice develop earlier onset and more rapid BMAT progression compared to other osteoporotic models, while the

expansion of BMAT was correlated with the levels of huRANKL and the severity of the osteoporotic phenotype. At the molecular level, TgRANKL femurs displayed high expression levels both for osteoclastic genes and osteoblastic markers, indicating increased bone remodelling, while adipogenic markers were also increased especially at the Tg5519 mice, supporting increased BM adipogenesis.

While osteoblasts and osteocytes are traditionally considered the primary source of RANKL (Nakashima et al., 2011), emerging evidence suggests that BMAdS produce RANKL and thereby promote osteoclastogenesis (Goto et al., 2011). Most recently, marrow adipogenic lineage precursors cells were identified to highly express RANKL contributing to bone resorption and bone remodeling (Hu et al., 2021). Furthermore, RANKL<sup>+</sup>/Pref-1<sup>+</sup> preadipocytes may influence the local bone microenvironment, promoting bone resorption (Takeshita et al., 2014). To investigate the cellular source of RANKL in TgRANKL femurs, we proceeded to fractionation of bones, BMAT and BM cells. Our expression analysis demonstrated that RANKL was predominantly expressed by the bone tissue and the BMAT fraction compared to BM cells, suggesting that BMAdS

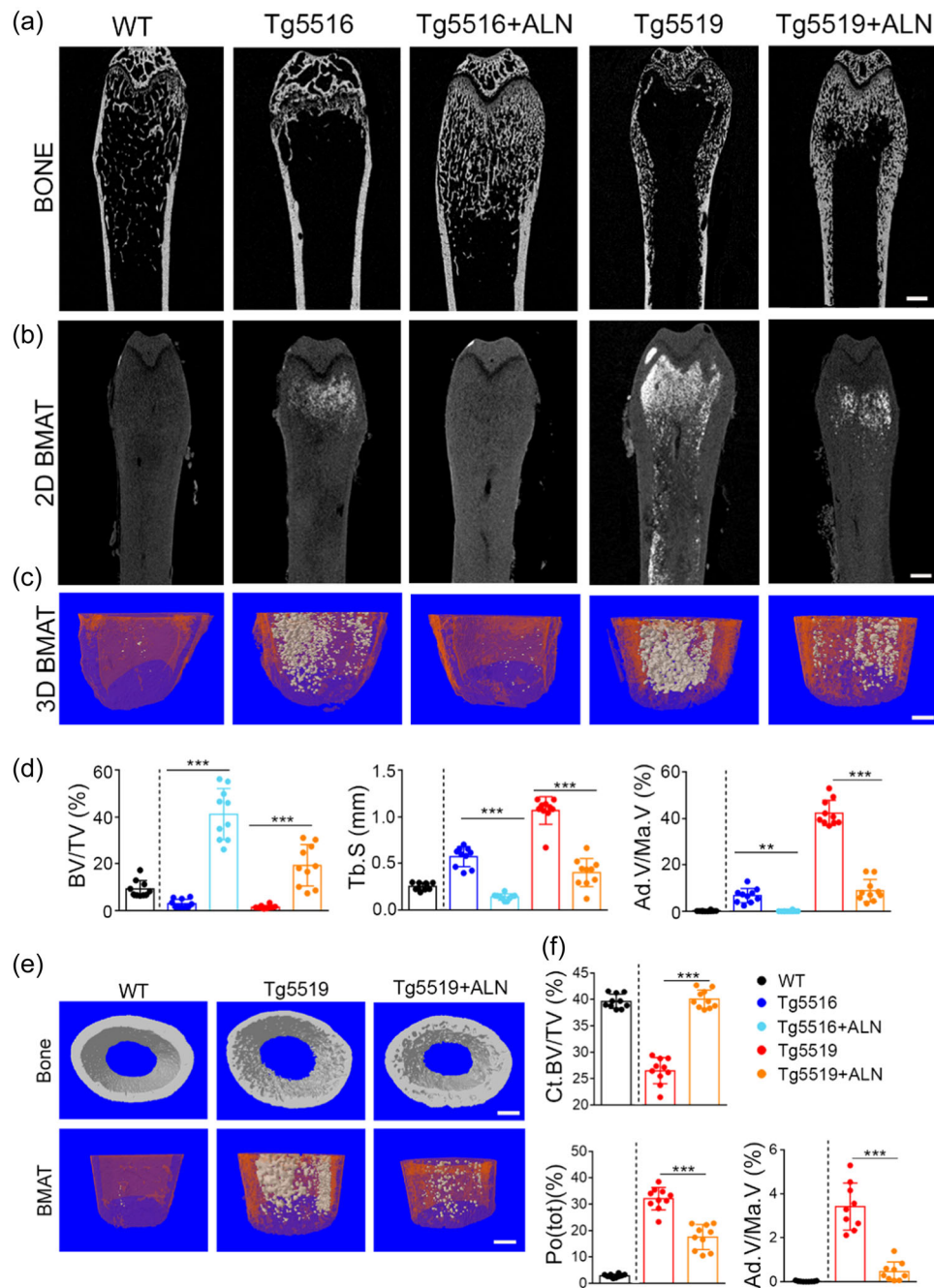


**FIGURE 5** Pharmacological inhibition of bone resorption attenuates bone marrow adipose tissue (BMAT) expansion in TgRANKL mice.

(a) Representative 2D microtomographic ( $\mu$ CT) images of distal femurs from Tg5516 and Tg5519 mice treated either with PBS or alendronate and wild-type (WT) littermates treated with PBS as controls; (b) Representative 2D and (c) 3D  $\mu$ CT images of BMAT upon osmium staining. Quantitative  $\mu$ CT analysis of (d) metaphyseal trabecular bone volume fraction (BV/TV, %), trabecular separation (Tb.S), and adipose volume fraction (Ad.V/Ma.V, %). (e) Representative 3D images of mid-diaphyseal cortical bone and BMAT, and (f) quantitative  $\mu$ CT analysis of cortical bone volume fraction (Ct. BV/TV, %), total porosity (Po(tot) %) and adipose volume fraction (Ad.V/Ma.V, %).  $n = 6-10$  mice per group, both sexes; scale bar = 500  $\mu$ m. Data are shown as mean values  $\pm$  SD. Two-way analysis of variance and Tukey post hoc test was performed for trabecular analysis while student's  $t$  test was performed for cortical analysis. WT mice were excluded from statistical analysis and separated from other groups using a vertical dot line in all presented graphs. PBS, phosphate-buffered saline. \*\* $p < 0.01$ , \*\*\* $p < 0.001$ .

constitute an important source of RANKL under osteoporotic conditions (Supporting Information S1: Figure S5). Similarly, high levels of RANKL were shown to be produced by BMAds in osteoporotic mice lacking PTH receptor in BMSCs (Fan et al., 2017) and ovariectomized C3H/HeJ mice (Beekman, Veldhuis-Vlug, et al., 2019). Despite the

widely documented positive association of increased BM fat content and bone loss in patients with primary osteoporosis as well as in aging individuals (Devlin & Rosen, 2015; Li et al., 2017), the role of RANKL expression by BMAds under conditions such as primary osteoporosis and aging remains elusive and needs further investigation. BMAT is

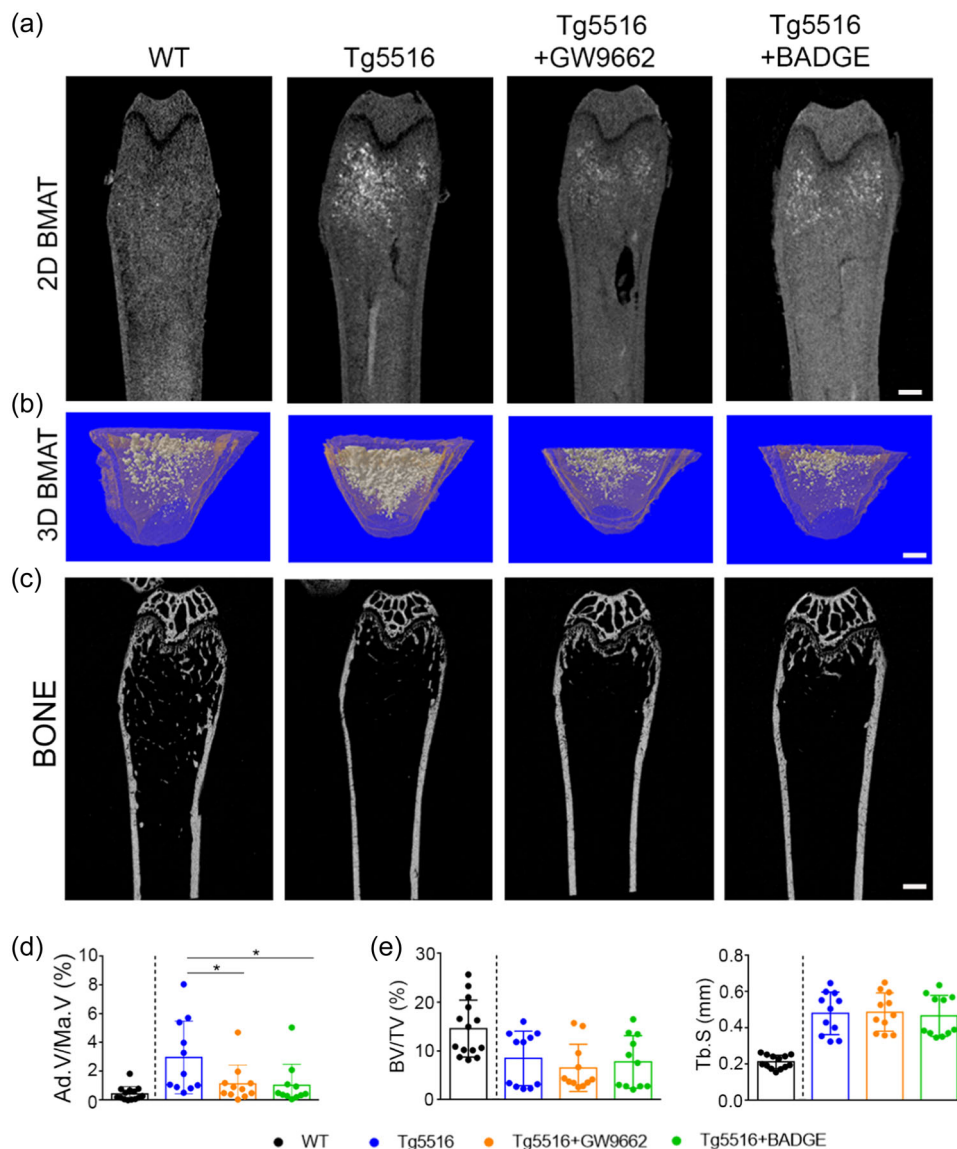


**FIGURE 6** Pharmacological inhibition of adipogenesis does not affect bone resorption in Tg5516 mice. (a) Representative 2D and (b) 3D microtomographic ( $\mu$ CT) images of bone marrow adipose tissue (BMAT) at the metaphyseal region from Tg5516 mice treated with GW9662 or BADGE. 15% DMSO in PBS (vehicle) was used in control wild-type (WT) and Tg5516 mice; (c) Representative 2D  $\mu$ CT images of distal femurs; (d) Quantitation of BMAT with  $\mu$ CT at the metaphyseal region, Ad.V/Ma.V (Adipose Volume/Marrow Volume, %). (e) Quantitative  $\mu$ CT analysis in metaphyseal trabecular bone of distal femurs from the above groups, BV/TV (Bone Volume/Total Volume, %), Tb.S (Trabecular Separation, mm).  $n = 11$ – $14$  mice per group, both sexes; scale bar =  $500 \mu\text{m}$ . Data are shown as mean values  $\pm$  SD. One-way analysis of variance and Dunnett's post hoc test was performed for statistical analysis. WT mice were excluded from statistical analysis and separated from other groups using a vertical dot line in all presented graphs. PBS, phosphate-buffered saline. \* $p < 0.05$ .

considered to be an endocrine organ that secretes various factors designated as adipokines including adiponectin, leptin, TNF, IL-6, as well as RANKL which affect bone homeostasis through the regulation of osteoblasts and osteoclasts (Herrmann, 2019). The co-progression of BMAT with bone resorption may indicate a mechanistic link between adipocytes and osteoclasts. Therefore, BMAT could regulate and promote osteoclastogenesis either directly through RANKL production or indirectly through other factors such as adiponectin, which stimulates osteoblasts to produce RANKL (Wang et al., 2014). However, an interesting aspect not addressed in

the current study is whether adipocyte-derived RANKL is directly involved in BM adipogenesis. Exploring this possibility could provide valuable insights into the specific roles of RANKL within the BM microenvironment, particularly in relation to adipocyte differentiation. Further investigations are needed to determine if RANKL produced by BMAd has a direct autocrine or paracrine effect on BM adipogenesis or if its influence is primarily indirect, mediated through changes in the bone niche or osteoclast activity.

To identify whether BMAT formation precedes or follows bone loss, we examined the progression of both phenomena in TgRANKL mice. Our

results showed that Tg5519 mice developed an early onset of trabecular bone loss and cortical porosity by the age of 4 weeks, without any evidence for presence of BMAT, suggesting that BMAT follows bone loss in this osteoporotic model. These findings were further supported by higher expression levels of osteoclastic genes but not of adipogenic genes in 4-week-old Tg5519 mice compared to WT controls. Thus, these results are consistent with the hypothesis that osteoclasts promote BMAT formation. To shed light under this scenario, we conducted co-culture experiments of isolated BMSCs from WT and Tg5519 and stimulated them with osteoclast-conditioned medium (OCM) under adipogenic conditions. Foremost, Tg5519 BMSCs displayed an increased adipogenic differentiation capacity which operates at the expense of osteogenesis compared to WT BMSCs. Notably, stimulation of WT and Tg5519 BMSCs with OCM under adipogenic conditions (1:1 ratio) resulted in an exaggerated adipogenic potential compared to nonstimulated ones. Such initial results should be substantiated by further studies to delineate and validate osteoclast-derived factors as potential inducers of BM adipogenesis.

To examine the *in vivo* effect of osteoclast inhibition in BMAT expansion, TgRANKL mice were treated with ALN, a bisphosphonate inhibitor of osteoclast activity (Fisher et al., 1999). Prophylactic treatment of Tg5516 mice with ALN not only protected from bone loss but also completely inhibited BMAT formation. In addition, therapeutic ALN administration in the severe osteoporosis model Tg5519 resulted in partial improvement of bone architecture and attenuation of BMAT expansion, suggesting that osteoclast may influence BMSC differentiation by releasing factors that promote adipogenic differentiation or by modulating the balance of other regulatory signals (Supporting Information S1: Figure S5). In accordance with our results, early treatment of ovariectomized rats with zoledronic acid, another bisphosphonate, has been found to fully preserve bone microarchitecture and reverse BMA (Li, Xu, Chang, et al., 2014).

The role of BMAT in mediating bone loss in osteoporosis is not fully clarified. To explore the effects of BMAT in bone loss, TgRANKL mice were treated with two known PPAR $\gamma$  antagonists, BADGE and GW9662, which attenuate adipocyte differentiation (Beekman, Veldhuis-Vlug, et al., 2019; Duque et al., 2013). Our data demonstrated that treatment of Tg5516 mice either with BADGE or GW9662 effectively attenuated BMAT expansion but could not affect bone loss, suggesting that BMAT is dispensable for bone resorption in this osteoporosis model. Interestingly, our data are in line with previous studies demonstrating that BADGE treatment, although effectively ameliorated BMAT, failed to strengthen bone mass in bone loss models (Botolin & McCabe, 2006; Li et al., 2016). Furthermore, a BMAT deficient genetic mouse model developed bone loss either after ovariectomy (Iwaniec & Turner, 2013), or in a disuse-induced bone loss model (Keune et al., 2017). Similarly, conditional deletion of PPAR $\gamma$  in mesenchymal progenitor cells prevented BMAT but failed to attenuate rosiglitazone-induced bone loss and age-related bone loss (Almeida et al., 2020).

In conclusion, despite the expression of RANKL by BMAds, our *in vivo* experimental system demonstrated that the suppression of BM adipogenesis did not affect bone resorption, which appears

intriguing given RANKL's established role in osteoclast differentiation. This apparent contradiction may be explained by the presence of alternative sources of RANKL, such as osteocytes and osteoblasts, which are sufficient to induce osteoclastogenesis and drive bone resorption independently of BMAd-derived RANKL. Conversely, our *in vivo* results demonstrated that inhibiting osteoclasts protected TgRANKL mice from both bone loss and BMAT expansion, highlighting the critical role of osteoclasts in BMAT expansion. Future studies should focus on elucidating the factors and mechanisms that mediate the interplay between osteoclasts and BMAT, and the TgRANKL model could offer further insights into the regulatory mechanisms coordinating BMAT accumulation and bone resorption.

## AUTHOR CONTRIBUTIONS

Eleni Douni conceived, guided and supervised this work. Eleni Douni and Vagelis Rinotas designed the experiments. Vagelis Rinotas, Efthymios Tzortzis, Konstantinos Kritikos, Panagiota Siatra, Apostolos Papadopoulos, Vasiliki-Iris Perivolidi and Evi Gkikopoulou conducted the experiments and analysed the data. Vagelis Rinotas and Eleni Douni wrote and revised the manuscript.

## ACKNOWLEDGEMENTS

We would like to thank the  $\mu$ CT facility at the B.S.R.C. "Al. Fleming" for performing the  $\mu$ CT scans. This research has been co-financed by the European Union and Greek national funds through the Operational Program Competitiveness, Entrepreneurship and Innovation under the call RESEARCH—CREATE—INNOVATE (Project code: T1EDK-02829). The publication of the article in OA mode was financially supported by HEAL-Link.

## CONFLICT OF INTEREST STATEMENT

The authors declare no conflict of interest.

## DATA AVAILABILITY STATEMENT

The data that support the findings of this study are available from the corresponding author upon reasonable request.

## ETHICS STATEMENT

All experimental protocols were performed with the approval of the Institutional Protocol Evaluation Committee and were licensed by the Veterinary Authorities of Attica Prefecture (registered code: 2201/11-04-2017) in compliance with the animal welfare guidelines of the PD 56/2013 and the European Directive 2010/63/EU.

## ORCID

Eleni Douni  <http://orcid.org/0000-0003-0004-5121>

## REFERENCES

- Abdallah, B. M., & Kassem, M. (2012). New factors controlling the balance between osteoblastogenesis and adipogenesis. *Bone*, 50(2), 540–545. <https://doi.org/10.1016/j.bone.2011.06.030>
- Almeida, M., Kim, H. N., Han, L., Zhou, D., Thostenson, J., Porter, R. M., Ambrogini, E., Manolagas, S. C., & Jilka, R. L. (2020). Increased marrow adipogenesis does not contribute to age-dependent

- appendicular bone loss in female mice. *Aging Cell*, 19(11), e13247. <https://doi.org/10.1111/acer.13247>
- Beekman, K. M., Veldhuis-Vlug, A. G., van der Veen, A., den Heijer, M., Maas, M., Kerckhofs, G., Parac-Vogt, T. N., Bisschop, P. H., & Bravenboer, N. (2019). The effect of PPAR $\gamma$  inhibition on bone marrow adipose tissue and bone in C3H/HeJ mice. *American Journal of Physiology—Endocrinology and Metabolism*, 316(1), E96–E105. <https://doi.org/10.1152/ajpendo.00265.2018>
- Beekman, K. M., Zwaagstra, M., Veldhuis-Vlug, A. G., Van Essen, H. W., Den Heijer, M., Maas, M., Kerckhofs, G., Parac-Vogt, T. N., Bisschop, P. H., & Bravenboer, N. (2019). Ovariectomy increases RANKL protein expression in bone marrow adipocytes of C3H/HeJ mice. *American Journal of Physiology—Endocrinology and Metabolism*, 317(6), E1050–E1054. <https://doi.org/10.1152/ajpendo.00142.2019>
- Botolin, S., & McCabe, L. R. (2006). Inhibition of PPAR $\gamma$  prevents type I diabetic bone marrow adiposity but not bone loss. *Journal of Cellular Physiology*, 209(3), 967–976. <https://doi.org/10.1002/jcp.20804>
- Bouxsein, M. L., Boyd, S. K., Christiansen, B. A., Gulberg, R. E., Jepsen, K. J., & Müller, R. (2010). Guidelines for assessment of bone microstructure in rodents using micro-computed tomography. *Journal of Bone and Mineral Research*, 25(7), 1468–1486. <https://doi.org/10.1002/jbmr.141>
- Bravenboer, N., Bredella, M. A., Chauveau, C., Corsi, A., Douni, E., Ferris, W. F., Riminucci, M., Robey, P. G., Rojas-Sutterlin, S., Rosen, C., Schulz, T. J., & Cawthorn, W. P. (2020). Standardised nomenclature, abbreviations, and units for the study of bone marrow adiposity: Report of the nomenclature working group of the international bone marrow adiposity society. *Frontiers in Endocrinology*, 10, 923. <https://doi.org/10.3389/fendo.2019.00923>
- Bucay, N., Sarosi, I., Dunstan, C. R., Morony, S., Tarpley, J., Capparelli, C., Scully, S., Tan, H. L., Xu, W., Lacey, D. L., Boyle, W. J., & Simonet, W. S. (1998). Osteoprotegerin-deficient mice develop early onset osteoporosis and arterial calcification. *Genes & Development*, 12(9), 1260–1268. <https://doi.org/10.1101/gad.12.9.1260>
- Devlin, M. J., & Rosen, C. J. (2015). The bone-fat interface: Basic and clinical implications of marrow adiposity. *The Lancet. Diabetes & Endocrinology*, 3(2), 141–147. [https://doi.org/10.1016/S2213-8587\(14\)70007-5](https://doi.org/10.1016/S2213-8587(14)70007-5)
- Douni, E., Rinotas, V., Makrinou, E., Zwerina, J., Penninger, J. M., Eliopoulos, E., Schett, G., & Kollias, G. (2012). A RANKL G278R mutation causing osteopetrosis identifies a functional amino acid essential for trimer assembly in RANKL and TNF. *Human Molecular Genetics*, 21(4), 784–798. <https://doi.org/10.1093/hmg/ddr510>
- Duque, G., Li, W., Adams, M., Xu, S., & Phipps, R. (2011). Effects of risendronate on bone marrow adipocytes in postmenopausal women. *Osteoporosis International*, 22(5), 1547–1553. <https://doi.org/10.1007/s00198-010-1353-8>
- Duque, G., Li, W., Vidal, C., Bermeo, S., Rivas, D., & Henderson, J. (2013). Pharmacological inhibition of PPAR $\gamma$  increases osteoblastogenesis and bone mass in male C57BL/6 mice. *Journal of Bone and Mineral Research*, 28(3), 639–648. <https://doi.org/10.1002/jbmr.1782>
- Fan, Y., Hanai, J., Le, P. T., Bi, R., Maridas, D., DeMambro, V., Figueroa, C. A., Kir, S., Zhou, X., Mannstadt, M., Baron, R., Bronson, R. T., Horowitz, M. C., Wu, J. Y., Bilezikian, J. P., Dempster, D. W., Rosen, C. J., & Lanske, B. (2017). Parathyroid hormone directs bone marrow mesenchymal cell fate. *Cell Metabolism*, 25(3), 661–672. <https://doi.org/10.1016/j.cmet.2017.01.001>
- Fisher, J. E., Rogers, M. J., Halasy, J. M., Luckman, S. P., Hughes, D. E., Masarachia, P. J., Wesolowski, G., Russell, R. G. G., Rodan, G. A., & Reszka, A. A. (1999). Alendronate mechanism of action: geranylgeraniol, an intermediate in the mevalonate pathway, prevents inhibition of osteoclast formation, bone resorption, and kinase activation in vitro. *Proceedings of the National Academy of Sciences*, 96, 133–138. <https://doi.org/10.1073/pnas.96.1.133>
- Fuller, K., Wong, B., Fox, S., Choi, Y., & Chambers, T. J. (1998). TRANCE is necessary and sufficient for osteoblast-mediated activation of bone resorption in osteoclasts. *The Journal of Experimental Medicine*, 188(5), 997–1001. <https://doi.org/10.1084/jem.188.5.997>
- Ghali, O., Broux, O., Falgayrac, G., Haren, N., van Leeuwen, J. P., Penel, G., Hardouin, P., & Chauveau, C. (2015). Dexamethasone in osteogenic medium strongly induces adipocyte differentiation of mouse bone marrow stromal cells and increases osteoblast differentiation. *BMC Cell Biology*, 16, 9. <https://doi.org/10.1186/s12860-015-0056-6>
- Goto, H., Hozumi, A., Osaki, M., Fukushima, T., Sakamoto, K., Yonekura, A., Tomita, M., Furukawa, K., Shindo, H., & Baba, H. (2011). Primary human bone marrow adipocytes support TNF- $\alpha$ -induced osteoclast differentiation and function through RANKL expression. *Cytokine*, 56(3), 662–668. <https://doi.org/10.1016/j.cyto.2011.09.005>
- Gullberg, B., Johnell, O., & Kanis, J. A. (1997). World-wide projections for hip fracture. *Osteoporosis International*, 7(5), 407–413. <https://doi.org/10.1007/PL00004148>
- Herrmann, M. (2019). Marrow fat-secreted factors as biomarkers for osteoporosis. *Current Osteoporosis Reports*, 17(Issue 6), 429–437. <https://doi.org/10.1007/s11914-019-00550-w>
- Hu, Y., Li, X., Zhi, X., Cong, W., Huang, B., Chen, H., Wang, Y., Li, Y., Wang, L., Fang, C., Guo, J., Liu, Y., Cui, J., Cao, L., Weng, W., Zhou, Q., Wang, S., Chen, X., & Su, J. (2021). RANKL from bone marrow adipose lineage cells promotes osteoclast formation and bone loss. *EMBO Reports*, 22(7), e52481. <https://doi.org/10.15252/embr.202152481>
- Iwaniec, U. T., & Turner, R. T. (2013). Failure to generate bone marrow adipocytes does not protect mice from ovariectomy-induced osteopenia. *Bone*, 53(1), 145–153. <https://doi.org/10.1016/j.bone.2012.11.034>
- Karsenty, G., & Wagner, E. F. (2002). Reaching a genetic and molecular understanding of skeletal development. *Developmental Cell*, 2(4), 389–406. [https://doi.org/10.1016/S1534-5807\(02\)00157-0](https://doi.org/10.1016/S1534-5807(02)00157-0)
- Keune, J. A., Wong, C. P., Branscum, A. J., Iwaniec, U. T., & Turner, R. T. (2017). Bone marrow adipose tissue deficiency increases disuse-induced bone loss in male mice. *Scientific Reports*, 7, 46325. <https://doi.org/10.1038/srep46325>
- Lacey, D. L., Timms, E., Tan, H. L., Kelley, M. J., Dunstan, C. R., Burgess, T., Elliott, R., Colombero, A., Elliott, G., Scully, S., Hsu, H., Sullivan, J., Hawkins, N., Davy, E., Capparelli, C., Eli, A., Qian, Y. X., Kaufman, S., Sarosi, I., ... Boyle, W. J. (1998). Osteoprotegerin ligand is a cytokine that regulates osteoclast differentiation and activation. *Cell*, 93(2), 165–176. [https://doi.org/10.1016/S0092-8674\(00\)81569-X](https://doi.org/10.1016/S0092-8674(00)81569-X)
- Li, G., Xu, Z., Hou, L., Li, X., Li, X., Yuan, W., Polat, M., & Chang, S. (2016). Differential effects of bisphenol A diglycidyl ether on bone quality and marrow adiposity in ovary-intact and ovariectomized rats. *American Journal of Physiology - Endocrinology and Metabolism*, 311(6), E922–E927. <https://doi.org/10.1152/ajpendo.00267.2016>
- Li, G. W., Xu, Z., Chang, S. X., Zhou, L., Wang, X. Y., Nian, H., & Shi, X. (2014). Influence of early zoledronic acid administration on bone marrow fat in ovariectomized rats. *Endocrinology*, 155(12), 4731–4738. <https://doi.org/10.1210/en.2014-1359>
- Li, G. W., Xu, Z., Chen, Q. W., Tian, Y. N., Wang, X. Y., Zhou, L., & Chang, S. X. (2014). Quantitative evaluation of vertebral marrow adipose tissue in postmenopausal female using MRI chemical shift-based water-fat separation. *Clinical Radiology*, 69(3), 254–262. <https://doi.org/10.1016/j.crad.2013.10.005>
- Li, J., Lu, L., Liu, L., Wang, C., Xie, Y., Li, H., Tian, L., & Yu, X. (2023). The unique role of bone marrow adipose tissue in ovariectomy-induced bone loss in mice. *Endocrine*, 83, 77–91. <https://doi.org/10.1007/s12020-023-03504-6>
- Li, X., Shet, K., Xu, K., Rodríguez, J. P., Pino, A. M., Kurhanewicz, J., Schwartz, A., & Rosen, C. J. (2017). Unsaturation level decreased in bone marrow fat of postmenopausal women with low bone density using high resolution magic angle spinning (HRMAS)1H NMR spectroscopy. *Bone*, 105, 87–92. <https://doi.org/10.1016/j.bone.2017.08.014>
- Marcadet, L., Bouredji, Z., Argaw, A., & Frenette, J. (2022). The roles of RANK/RANKL/OPG in cardiac, skeletal, and smooth muscles in health and disease. *Frontiers in Cell and Developmental Biology*, 10, 903657. <https://doi.org/10.3389/fcell.2022.903657>

- Nakashima, T., Hayashi, M., Fukunaga, T., Kurata, K., Oh-hora, M., Feng, J. Q., Bonewald, L. F., Kodama, T., Wutz, A., Wagner, E. F., Penninger, J. M., & Takayanagi, H. (2011). Evidence for osteocyte regulation of bone homeostasis through RANKL expression. *Nature Medicine*, 17(10), 1231–1234. <https://doi.org/10.1038/nm.2452>
- Rendina-Ruedy, E., & Rosen, C. J. (2020). Lipids in the bone marrow: an evolving perspective. *Cell Metabolism*, 31(2), 219–231. <https://doi.org/10.1016/j.cmet.2019.09.015>
- Rinotas, V., Niti, A., Dacquin, R., Bonnet, N., Stolina, M., Han, C.-Y., Kostenuik, P., Jurdic, P., Ferrari, S., & Douni, E. (2014). Novel genetic models of osteoporosis by overexpression of human RANKL in transgenic mice. *Journal of Bone and Mineral Research*, 29(5), 1158–1169. <https://doi.org/10.1002/jbmr.2112>
- Rosen, C. J., & Bouxsein, M. L. (2006). Mechanisms of disease: Is osteoporosis the obesity of bone? *Nature Clinical Practice. Rheumatology*, 2(1), 35–43. <https://doi.org/10.1038/ncprheum0070>
- Scheller, E. L., Troiano, N., Vanhoutan, J. N., Bouxsein, M. A., Fretz, J. A., Xi, Y., Nelson, T., Katz, G., Berry, R., Church, C. D., Doucette, C. R., Rodeheffer, M. S., MacDougald, O. A., Rosen, C. J., & Horowitz, M. C. (2014). Use of osmium tetroxide staining with microcomputerized tomography to visualize and quantify bone marrow adipose tissue in vivo. *Methods in Enzymology*, 537, 123–139. <https://doi.org/10.1016/B978-0-12-411619-1.00007-0>
- Takeshita, S., Fumoto, T., Naoe, Y., & Ikeda, K. (2014). Age-related marrow adipogenesis is linked to increased expression of RANKL. *Journal of Biological Chemistry*, 289(24), 16699–16710. <https://doi.org/10.1074/jbc.M114.547919>
- Tratwal, J., Rojas-Sutterlin, S., Bataclan, C., Blum, S., & Naveiras, O. (2021). Bone marrow adiposity and the hematopoietic niche: A historical perspective of reciprocity, heterogeneity, and lineage commitment. *Best Practice & Research Clinical Endocrinology & Metabolism*, 35(4), 101564. <https://doi.org/10.1016/j.beem.2021.101564>
- Wang, Q., Li, X., Wang, M., Zhao, L., Li, H., Xie, H., & Lu, Z. (2014). Adiponectin exerts its negative effect on bone metabolism via OPG/RANKL pathway: An in vivo study. *Endocrine*, 47(3), 845–853. <https://doi.org/10.1007/s12020-014-0216-z>
- Yang, Y., Luo, X., Yan, F., Jiang, Z., Li, Y., Fang, C., & Shen, J. (2015). Effect of zoledronic acid on vertebral marrow adiposity in postmenopausal osteoporosis assessed by MR spectroscopy. *Skeletal Radiology*, 44(10), 1499–1505. <https://doi.org/10.1007/s00256-015-2200-y>
- Zhang, L., Liu, M., Zhou, X., Liu, Y., Jing, B., Wang, X., Zhang, Q., & Sun, Y. (2016). Role of osteoprotegerin (OPG) in bone marrow adipogenesis. *Cellular Physiology and Biochemistry*, 40(3–4), 681–692. <https://doi.org/10.1159/000452580>
- Zhang, Y., Chen, S. E., Shao, J., & Van Den Beucken, J. P. (2018). Combinatorial surface roughness effects on osteoclastogenesis and osteogenesis. *ACS Applied Materials & Interfaces*, 10(43), 36652–36663. <https://doi.org/10.1021/acsami.8b10992>

## SUPPORTING INFORMATION

Additional supporting information can be found online in the Supporting Information section at the end of this article.

**How to cite this article:** Rinotas, V., Gkikopoulou, E., Tzortzis, E., Kritikos, K., Siatra, P., Papadopoulos, A., Perivolidi, V.-I., & Douni, E. (2024). Interplay between bone marrow adiposity and bone resorption in RANKL-mediated modelled osteoporosis. *Journal of Cellular Physiology*, 239, e31434. <https://doi.org/10.1002/jcp.31434>